Optics Letters

Rapid acquisition of broadband two-dimensional electronic spectra by continuous scanning with conventional delay lines

Austin P. Spencer* and Lin X. Chen

Department of Chemistry, Northwestern University, Evanston, Illinois 60208-3113, USA
**Corresponding author: Austin. Spencer@northwestern.edu*

Received 26 February 2020; revised 17 April 2020; accepted 24 April 2020; posted 27 April 2020 (Doc. ID 391360); published 15 May 2020

A passively phase-stable, broadband (~7 fs, >2000 cm^{-1}) two-dimensional (2D) electronic spectroscopy apparatus that achieves rapid acquisition rates by continuously—rather than step-wise—scanning the Fourier-transform dimension is demonstrated for the first time, to the best of our knowledge. This is made possible through use of a partially common path interferometer design in which the coherence time τ is sampled in a "rotating frame." Rapid, continuous scanning of τ increases the duty cycle of signal collection, rejects the majority of excitation pulse scatter, and enables the measurement of a complete 2D spectrum in 92 ms, which minimizes the influence of pulse intensity and delay fluctuations on the 2D spectrum. In practice, these improvements make possible the acquisition of hundreds of 2D spectra in tens of minutes, which opens the door to dense sampling of ultrafast relaxation dynamics and to generating extremely broadband 3D Fourier-transform spectra.

https://doi.org/10.1364/OL.391360

Two-dimensional electronic spectroscopy [1,2] (2DES) is a powerful method for exploring the electronic and vibrational dynamics of molecules [3–5], proteins [6,7], and materials [8,9]. Compared to transient absorption (TA) spectroscopy [10], 2DES enables higher time resolution and broader bandwidth. By resolving spectral features over two frequency dimensions, electronic state coupling and relaxation dynamics are more easily and accurately extracted. Along with the additional information in 2DES comes additional experimental complexity, due primarily to the need for interferometric stability and control of the excitation pulse delays and for phase-sensitive detection of the signal field. Additionally, the need to resolve the signal field along two time–frequency dimensions increases the scale of data collection. The requirement for interferometric stability has been addressed through various approaches, including active phase stabilization [11–13], passive phase stabilization [14–17], and spatial multiplexing [18,19], each with its own advantages and disadvantages. Likewise, more rapid and efficient methods for collecting the two distinct time–frequency dimensions in 2DES have been developed, such as rapid pulse shaping [20,21] and spatial multiplexing [7,18]. Unfortunately, many of the solutions to these problems are either too complex or impractical for very broadband visible laser sources for which temporal, spatial, and angular dispersion are difficult to avoid. Here, we present a 2DES method that achieves both high phase stability and rapid acquisition speed using only conventional optics.

2DES utilizes a "pump" pulse pair (pulses 1 and 2) to excite the sample followed by a "probe" pulse (pulse 3) to detect changes in the sample's optical properties. The emitted signal field's spectrum and phase are characterized (typically using spectral interferometry [22] [SI]) at a range of coherence time delays τ between the pump pulses. The signal field is Fourier transformed along τ to yield the 2D spectrum as a function of the pump "excitation" (ω_τ) and probe "detection" (ω_τ) frequencies.

Since the signal field's phase is interferometrically sensitive to τ, it is typically necessary to sample τ discretely at <1 fs (sub-Nyquist) steps. This is often achieved in a step-wise process by moving the τ delay line to a stationary point, acquiring the signal field interferogram, and then repeating for all desired τ points. Unfortunately, this method is slow and has a low duty cycle of data collection, leading to long acquisition times and reduced signal-to-noise.

To overcome these limitations, we combine two experimental advances that significantly shorten the time needed to acquire a 2D spectrum: (1) a partially common path interferometer design and (2) rapid, continuous delay scanning. The advantages of using a partially common path design for passive phase stability in multidimensional spectroscopy have been well documented [14,15,23,24]. However, this design also allows for sampling the τ dimension in a frame of reference that rotates synchronously at ω_t. In such a quasi-rotating frame (QRF), the linear component $\omega_\tau \tau$ of the signal phase is approximately cancelled, reducing the apparent center frequency of the signal along τ to zero. QRF acquisition greatly relaxes the sampling requirements along τ since the Nyquist rate of the signal is reduced approximately by the ratio of the signal's bandwidth to its center frequency, a property that has been exploited in 2D infrared (IR) spectroscopy [25] and 2DES [23].

Rapid delay scanning involves continuously sweeping (rather than step-wise sampling) τ during data acquisition, thereby increasing the speed of data collection. Critically, by shortening the total time needed to acquire a complete 2D spectrum to 92 ms, the influence of $1/f$ noise sources is greatly reduced. Rapid scanning along τ is possible due to the reduction in apparent signal frequency along τ afforded by QRF acquisition. Otherwise, continuous delay stage motion would cause the signal–local oscillator (LO) interferograms to be blurred due to integration over the typical $\omega_\tau \tau$ phase evolution of the signal during each camera exposure. In contrast, QRF acquisition is not necessary in rapid scanning implementations for 2D IR [26,27] and 2D vibrational–electronic [28] spectroscopies for which the lower frequency of IR light allows for integration over relatively large ranges of τ without attenuating the spectral interference.

The laser source for this instrument is a 10 kHz repetition rate Ti:Sapph regeneratively amplified laser system (Spectra-Physics, Solstice Ace). The 35 fs pulses from the amplifier seed a second-harmonic-pumped, noncollinear optical parametric amplifier (NOPA) (home-built) that generates 2.5 μJ pulses spanning 500–720 nm of instantaneous bandwidth [29]. The NOPA output pulses are compressed and characterized using multiphoton intrapulse interference phase scan (MIIPS) with a 4-f pulse shaper (Biophotonics, MIIPSBox640), yielding 5–7 fs, 400 nJ pulses. As depicted in Fig. 1, the input beam to the apparatus is first split by a dielectric beam splitter (Layertec, 106896) into two beams: one transmitted that will yield pulses 1 and 3 and one reflected that will yield pulses 2 and 4. These two beams travel down their respective delay lines, are reflected by hollow corner-cube retroreflectors (PLX, OW-25-30-E), and return to vertically offset points near the beam splitter. The reflected path contains a compensating block (Thorlabs, WG41010) (i.e., window) of thickness matched to that of the beam splitter and rotated by 45° vertically to take advantage of reduced reflection for p polarization near Brewster's angle. The retroreflector for the transmitted path (pulses 1 and 3) translates the beam down and is mounted on a linear motor translation stage (Newport, XMS50-S) [blue rectangle labeled α in Fig. 1] that allows for precise nm-scale control of the delay line path length. Starting from equal path lengths and extending the delay line path for pulses 1 and 3 by length $2\Delta\ell_\alpha$ (corresponding to a $\Delta\ell_\alpha$ retreat of the retroreflector) adds a delay of $\Delta t_\alpha = 2\Delta\ell_\alpha/c$ relative to pulses 2 and 4. The two beams return from the retroreflectors to a mirror that reflects the beam containing pulses 1 and 3 while permitting the beam containing pulses 2 and 4 to pass above, ultimately forming a vertically stacked, parallel beam arrangement. This set of two beams is then split by a single dielectric beam splitter into two pairs of beams: one pair containing pulses 1 and 2 and one pair containing pulses 3 and 4. As before, the two pairs of beams travel down their respective delay lines, with a compensating block (Thorlabs, WG41010R) in the reflected path, and are reflected by hollow corner-cube retroreflectors. Pulse 4, which ultimately serves as the LO for SI, transmits through a reflective neutral density filter (Thorlabs, NDUV40A) and achromatic half-wave plate (Special Optics, 8-9015-1/2), with pulse 3 passing above these two optics. Similar to delay line α, the path length of delay line β (pulses 3 and 4) for the reflected beams is controlled by a linear motor translation stage, while the transmitted beam path is fixed. Extending the delay line path for pulses 3 and 4 by length $2\Delta\ell_\beta$ adds a delay of $\Delta t_\beta = 2\Delta\ell_\beta/c$.

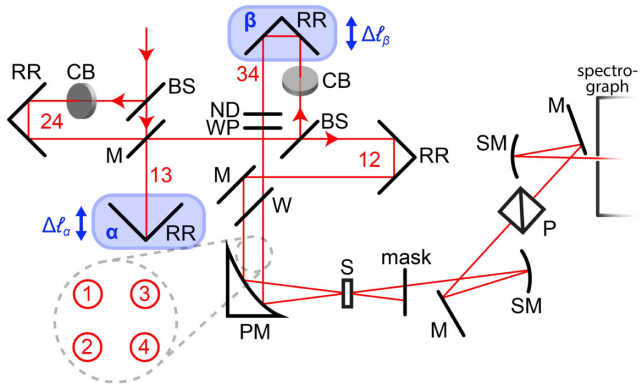

Fig. 1. Schematic of the optical apparatus. Beams are labeled by red numerals (1, 2, 3, 4) signifying which pulses they contain. Motorized translation stages are indicated by blue boxes under the retroreflectors that they control. A close-up view (dashed-line call-out) of the beam arrangement prior to the parabolic mirror shows the square BOXCARS geometry employed in this apparatus. M, mirror; RR, retroreflector; BS, beam splitter; CB, compensating block; W, window; ND, neutral density filter; WP, half-wave plate; PM, parabolic mirror; S, sample; SM, spherical mirror; P, polarizer.

A mirror combines the two pairs of stacked beams into a horizontally offset arrangement, forming the square BOXCARS beam geometry shown in the inset of Fig. 1. A 1 mm thick fused silica window (Thorlabs, WG41010R) is placed at an angle in the path of pulses 1–3 (with pulse 4 passing by the side) to partially offset the delay of pulse 4 introduced by the neutral density filter and wave plate. A 15.2 cm focal length, 90° off-axis parabolic mirror (Thorlabs, MPD269-P01) focuses the four beams to a ∼40 μm common focal point in the sample cuvette with up to 70 nJ per excitation pulse. The signal and LO are isolated from the excitation pulses (pulses 1–3) by a spatial mask and are imaged from the sample focus to the spectrograph slit using a system of two spherical curved mirrors (300 mm and 100 mm focal lengths, respectively) and two flat mirrors. A Glan–Taylor calcite polarizer (Thorlabs, GT10) between the two flat mirrors rejects components of the LO and signal that are not polarized parallel to the excitation pulses (i.e., vertically). The LO intensity is adjusted by rotating the half-wave plate, which alters the LO polarization and therefore its transmission through the polarizer. The difference in total length traveled through glass and optics results in a delay of ∼1.2 ps for the LO relative to the excitation pulses. The signal–LO spectral interferogram is captured by a 300 mm spectrograph (Andor, Shamrock SR-303i) equipped with a 300 l/mm grating and an EMCCD image sensor (Andor, Newton). The amplitude and phase of the signal field are characterized using Fourier-transform SI [22].

Due to the coupling between pulse delays in the partially common path interferometer design, the delays τ and T are generally described by a system of equations involving both delay line time offsets Δt_α and Δt_β, which are positive when the movable delay line is lengthened. We define t_n to be the time of arrival to the sample of pulse n relative to pulse 3 (i.e., $t_3 = 0$) as a function of Δt_α and Δt_β such that $t_1 = -\Delta t_\beta$, $t_2 = -\Delta t_\alpha - \Delta t_\beta$, $t_4 = -\Delta t_\alpha + \Delta t_g$, where Δt_g is the delay introduced by the additional path through optics experienced

by the LO compared to the excitation pulses. We define the coherence time τ and relaxation time T as

$$\tau \equiv t_2 - t_1 = -\Delta t_\alpha, \tag{1}$$

$$T \equiv \min(|t_1|, |t_2|) = \min(|-\Delta t_\beta|, |-\Delta t_\alpha - \Delta t_\beta|). \tag{2}$$

For non-rephasing 2D spectra ($\tau \le 0$), $|t_1| < |t_2|$, and therefore Eq. (2) simplifies to $T = |-\Delta t_\beta|$. For rephasing 2D spectra ($\tau \ge 0$), $|t_1| > |t_2|$, and therefore Eq. (2) simplifies to $T = |-\Delta t_\alpha - \Delta t_\beta|$. Finally, solving Eqs. (1) and (2) for the experimentally controlled delays Δt_α and Δt_β in terms of τ and T yields

$$\Delta t_\alpha = -\tau, \tag{3}$$

$$\Delta t_\beta = \begin{cases} T + \tau & \text{if } \tau \ge 0 \text{ and } T \ge 0 \\ T & \text{if } \tau \le 0 \text{ and } T \ge 0. \end{cases} \tag{4}$$

Since pulses are delayed as pairs, τ cannot be varied without also varying the delay of the LO, which is given by $t_{\mathrm{LO}} \equiv t_4 = \tau + \Delta t_g$.

The signal field is characterized by Fourier-transform SI [22] using the LO pulse as a reference field. The Fourier transform of the real-valued time-domain electric field of a pulse $E(t)$ is given by $\hat{E}(\omega) = e(\omega)\exp[i\phi(\omega)]$, where $\hat{E}(\omega)$ is the complex-valued frequency-domain electric field, ω is angular frequency, $e(\omega)$ is the real-valued spectral envelope, and $\phi(\omega)$ is the spectral phase. From the spectral interferogram $I(\omega) = |\hat{E}_s(\omega) + \hat{E}_{\mathrm{LO}}(\omega)|^2$ between the signal $\hat{E}_s$ and LO $\hat{E}_{\mathrm{LO}}$ fields, we isolate the interference term

$$\hat{E}_s(\omega)\hat{E}^*_{\mathrm{LO}}(\omega) = e_s(\omega)e_{\mathrm{LO}}(\omega)\exp\{i[\Delta\phi_s(\omega) - \Delta\phi_{\mathrm{LO}}(\omega)]\}, \tag{5}$$

through Fourier filtering where $\Delta\phi_\gamma(\omega) = \phi_\gamma(\omega) - \phi_3(\omega)$ is the spectral phase of field γ ($= s$, LO, 1, 2, 3) relative to pulse 3. The phase of the LO field is related to its delay via

$$\Delta\phi_{\mathrm{LO}}(\omega) = \omega t_{\mathrm{LO}} = \omega\tau + \omega\Delta t_g. \tag{6}$$

The spectral phase of the signal field ϕ_s is proportional to the sum of the phases of the excitation pulses ϕ_n:

$$\Delta\phi_s(\omega_1, \omega_2, \omega_3) = \Delta\phi_1(-\omega_1) + \Delta\phi_2(\omega_2) + \Delta\phi_3(\omega_3)$$
$$= -\omega_1 t_1 + \omega_2 t_2, \tag{7}$$

where ω_n is the frequency of field–matter interaction with pulse n. In the limit that $\omega_1 = \omega_2 = \omega_3 = \omega_t$ and substituting from Eq. (1), the signal spectral phase can be simplified to

$$\Delta\phi_s(\omega_t) = \omega_t(t_2 - t_1) = \omega_t\tau. \tag{8}$$

Using Eqs. (6) and (8), the signal–LO phase difference in Eq. (5) becomes

$$\Delta\phi_s(\omega_t) - \Delta\phi_{\mathrm{LO}}(\omega_t) = -\omega_t\Delta t_g. \tag{9}$$

The signal–LO phase difference is independent of τ due to approximate cancellation of equal but opposite phase evolution of the signal during τ and t. In the limit that $-\omega_\tau = \omega_t$, the cancellation is exact. The practical consequence is that the interference pattern between the signal and LO fields does not appreciably shift with changes in τ, greatly reducing the requisite sampling frequency along τ since the signal is effectively measured in a QRF. Therefore, we can sample τ steps that are larger than the optical period (i.e., $\Delta\tau > 2\pi/\omega$) and can integrate spectral interferograms over a range of τ values without attenuating the spectral interference. The maximum τ step size is limited only by the spectral bandwidth of the signal along ω_τ and is independent of the excitation pulse wavelength.

In order to prevent Fourier-transform artifacts (such as ghosting due to unequal delay steps along τ) and to enable averaging of repeated measurements, spectral interferograms of the signal field must be acquired at accurate and repeatable values of τ. This is achieved by configuring the motorized translation stage responsible for scanning τ (delay line α, with pulses 1 and 3) to trigger the spectrograph camera at specific locations along its axis of travel. In this configuration, the delay line is continuously swept at a constant velocity through a range of positions that encompasses the set of requisite τ points such that spectral interferograms are accurately captured at the desired τ delays (confirmed by SI of pulses 1 and 2).

Equations (1) and (2) indicate that for *rephasing* 2D spectra, both delay lines are dependent on τ. Therefore, both delay lines must move in concert in order to maintain a fixed T delay while scanning τ. This is achieved by linking the two translation stages such that delay line β tracks the motion of delay line α, enforcing the relationship $\Delta\ell_\beta = -\Delta\ell_\alpha$. Alternatively, for non-rephasing 2D spectra ($\tau \le 0$), only the α delay line is dependent on τ, and so coordination of delay stage motion is not needed.

An additional benefit of continuous delay scanning is that the influence of scattered excitation light is greatly reduced, obviating the need for scatter subtraction by pump pulse chopping or phase cycling. For rephasing scans, spectral interference between the LO and scattered excitation light evolves in phase at the optical frequency along the scanned dimension. Therefore, when integrated over the delay range integrated in a single camera exposure, the interference between scatter and LO blurs out. During the subsequent Fourier filtering steps in data processing, these now spectrally smooth scatter components are rejected since they appear near zero frequency (DC).

A typical measurement of rephasing 2D spectra, composed of 26 τ points and acquired at 300 distinct T delays, requires 4–5 min, or approximately 1 s per T delay. Depending on the sample properties and excitation fluence, a sufficient signal-to-noise ratio for quantifying relaxation dynamics and vibrational beating signatures can be achieved by averaging three to 40 repeated T scans. Sampling τ at 5 fs intervals provides a $\sim$6700 cm^{-1} spectral range that is sufficient for use with our $\sim$7 fs excitation pulses. The phase of 2D spectra is corrected using the projection–slice theorem method [30,31] by comparing to TA spectra measured *in situ* after first subtracting the phase of a reference 2D spectrum of neat solvent [5] at $T = 0$.

Rephasing 2D spectra were measured for a zinc porphyrin (5, 15-bis[triisopropylsilylethynyl]-10, 20-di[3, 5-bis(3, 3-dimethylbutoxy)phenyl]porphinato)zinc(II) in solution at T delays from 50 fs to 3 ps in 8 fs steps with τ ranging from 0 fs to 120 fs in 5 fs steps using 7 nJ excitation pulses and 3 ms camera exposures. The complete T scan was repeated 20 times and averaged, yielding 2D spectra with standard deviation of the mean averaging 0.9% (3.5% max) in the real part and averaging 0.4% (1.3% max) in the absolute value. The real part of the rephasing

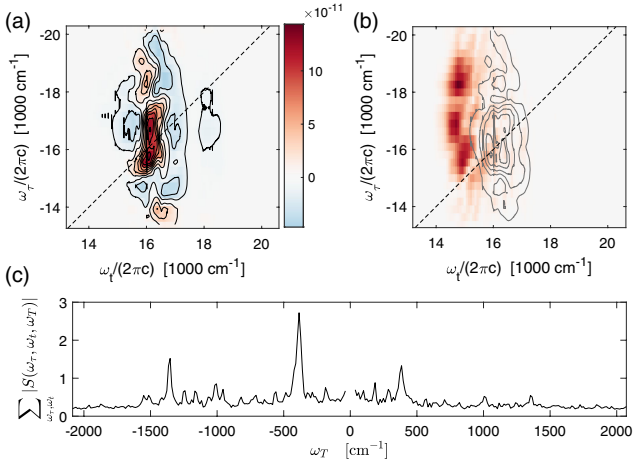

Fig. 2. 2DES data for excitation of the Q-band region of (5,15-bis[triisopropylsilylethynyl]-10, 20-di[3,5-bis(3, 3-dimethylbutoxy) phenyl]porphinato)zinc(II). (a) Real part of the rephasing 2D spectrum at $T = 1$ ps. (b) Beating map for $\omega_T = -1353\ \mathrm{cm}^{-1}$ with the absolute value rephasing 2D spectrum at $T = 1$ ps overlaid as gray contours. (c) Integrated beating spectrum.

2D spectrum for $T = 1$ ps is shown in Fig. 2(a). After population dynamics along T were globally modeled and subtracted, the 2DES data were Fourier transformed along T to form a 3D spectrum. Summing the absolute value of the 3D spectrum over ω_τ and ω_t yields the integrated beating spectrum in Fig. 2(c), which exhibits a broad range of vibrational resonances. Selecting the slice of the 3D spectrum at $\omega_T/2\pi c = -1353\ \mathrm{cm}^{-1}$ yields a beating map [Fig. 2(b)] that highlights the parts of the 2D spectrum that oscillate at the chosen frequency.

In summary, we have demonstrated a passively phase-stable 2DES instrument that enables rapid and efficient acquisition of 2D spectra. QRF acquisition enables undersampling of the signal field along τ, significantly reducing the number of τ samples necessary to fully capture the signal. The resultant reduction in data sampling burden allows for 2D spectra with the same signal-to-noise ratio to be measured much more rapidly. In practice, this yields at least a factor of five speed improvement for broadband visible 2DES. QRF acquisition also enables continuous scanning of the τ delay, which rejects the majority of excitation pulse scatter and nearly eliminates dead time between camera exposures during a τ scan, thereby increasing the rate of data acquisition. These speed improvements makes practical the dense T-delay sampling necessary to capture coherent oscillatory dynamics, which appear prevalent in energy and charge transfer processes. [32] Furthermore, compatibility with extremely broadband laser sources makes possible investigations into short-lived (<50 fs), high-frequency (>2000 cm^{-1}) coherent signatures that could yield insight into important processes such as singlet fission and ultrafast charge separation.

Funding. National Science Foundation (NSF CHE 1665021).

Acknowledgment. The authors thank Dr. Pyosang Kim for constructing and maintaining the laser source and Prof. Michael J. Therien for graciously providing the porphyrin sample.

Disclosures. The authors declare no conflicts of interest.

REFERENCES

1. J. D. Hybl, A. W. Albrecht, S. M. Gallagher Faeder, and D. M. Jonas, Chem. Phys. Lett. **297**, 307 (1998).
2. D. M. Jonas, Annu. Rev. Phys. Chem. **54**, 425 (2003).
3. J. D. Hybl, A. Yu, D. A. Farrow, and D. M. Jonas, J. Phys. Chem. A **106**, 7651 (2002).
4. A. Halpin, P. J. M. Johnson, R. Tempelaar, R. S. Murphy, J. Knoester, T. L. C. Jansen, and R. J. D. Miller, Nat. Chem. **6**, 196 (2014).
5. S. Irgen-Gioro, A. P. Spencer, W. O. Hutson, and E. Harel, J. Phys. Chem. Lett. **9**, 6077 (2018).
6. A. F. Fidler, V. P. Singh, P. D. Long, P. D. Dahlberg, and G. S. Engel, J. Chem. Phys. **139**, 155101 (2013).
7. A. P. Spencer, B. Spokoyny, and E. Harel, J. Phys. Chem. Lett. **6**, 945 (2015).
8. E. Vella, H. Li, P. Grégoire, S. M. Tuladhar, M. S. Vezie, S. Few, C. M. Bazán, J. Nelson, C. Silva-Acuña, and E. R. Bittner, Sci. Rep. **6**, 29437 (2016).
9. E. Cassette, R. D. Pensack, B. Mahler, and G. D. Scholes, Nat. Commun. **6**, 6086 (2015).
10. R. Berera, R. van Grondelle, and J. T. M. Kennis, Photosynth. Res. **101**, 105 (2009).
11. T. Zhang, C. Borca, X. Li, and S. Cundiff, Opt. Express **13**, 7432 (2005).
12. M. K. Yetzbacher, T. L. Courtney, W. K. Peters, K. A. Kitney, E. R. Smith, and D. M. Jonas, J. Opt. Soc. Am. B **27**, 1104 (2010).
13. W. Zhu, R. Wang, C. Zhang, G. Wang, Y. Liu, W. Zhao, X. Dai, X. Wang, G. Cerullo, S. Cundiff, and M. Xiao, Opt. Express **25**, 21115 (2017).
14. M. L. Cowan, J. P. Ogilvie, and R. J. D. Miller, Chem. Phys. Lett. **386**, 184 (2004).
15. U. Selig, F. Langhojer, F. Dimler, T. Löhrig, C. Schwarz, B. Gieseking, and T. Brixner, Opt. Lett. **33**, 2851 (2008).
16. Y. Zhang, K. Meyer, C. Ott, and T. Pfeifer, Opt. Lett. **38**, 356 (2013).
17. X. Ma, J. Dostál, and T. Brixner, Opt. Express **24**, 20781 (2016).
18. E. Harel, A. F. Fidler, and G. S. Engel, Proc. Natl. Acad. Sci. USA **107**, 16444 (2010).
19. A. P. Spencer, B. Spokoyny, S. Ray, F. Sarvari, and E. Harel, Nat. Commun. **7**, 10434 (2016).
20. W. Wagner, P. Tian, C. Li, J. Semmlow, and W. S. Warren, J. Mod. Opt. **51**, 2655 (2004).
21. N. M. Kearns, R. D. Mehlenbacher, A. C. Jones, and M. T. Zanni, Opt. Express **25**, 7869 (2017).
22. L. Lepetit, G. Chériaux, and M. Joffre, J. Opt. Soc. Am. B **12**, 2467 (1995).
23. L. A. Bizimana, J. Brazard, W. P. Carbery, T. Gellen, and D. B. Turner, J. Chem. Phys. **143**, 164203 (2015).
24. A. P. Spencer, W. O. Hutson, and E. Harel, Nat. Commun. **8**, 14732 (2017).
25. P. L. Kramer, C. H. Giammanco, A. Tamimi, D. J. Hoffman, K. P. Sokolowsky, and M. D. Fayer, J. Opt. Soc. Am. B **33**, 1143 (2016).
26. J. Helbing and P. Hamm, J. Opt. Soc. Am. B **28**, 171 (2011).
27. S. T. Roberts, J. J. Loparo, K. Ramasesha, and A. Tokmakoff, Opt. Commun. **284**, 1062 (2011).
28. Z. W. Fox, T. J. Blair, R. B. Weakly, T. L. Courtney, and M. Khalil, Rev. Sci. Instrum. **89**, 113104 (2018).
29. C. Manzoni, D. Polli, and G. Cerullo, Rev. Sci. Instrum. **77**, 023103 (2006).
30. J. D. Hybl, A. Albrecht Ferro, and D. M. Jonas, J. Chem. Phys. **115**, 6606 (2001).
31. V. P. Singh, A. F. Fidler, B. S. Rolczynski, and G. S. Engel, J. Chem. Phys. **139**, 084201 (2013).
32. G. D. Scholes, G. R. Fleming, L. X. Chen, A. Aspuru-Guzik, A. Buchleitner, D. F. Coker, G. S. Engel, R. van Grondelle, A. Ishizaki, D. M. Jonas, J. S. Lundeen, J. K. McCusker, S. Mukamel, J. P. Ogilvie, A. Olaya-Castro, M. A. Ratner, F. C. Spano, K. B. Whaley, and X. Zhu, Nature **543**, 647 (2017).